Electronic Supplementary Material (ESI) for Environmental Science: Nano.

Supporting Information

Metal-encapsulated carbon nanotube arrays for enhancing electrocatalytic nitrate reduction in wastewater: Importance of lying-down to standing-up structure transition

Yanyan Chen, Huanxin Ma, Weijian Duan*, Zichao Lin, Chunhua Feng*

The Key Lab of Pollution Control and Ecosystem Restoration in Industry Clusters, Ministry of Education, School of Environment and Energy, South China University of Technology, Guangzhou 510006, PR China

* Corresponding author. Tel.: +86-20-39380588; Fax: +86-20-39380588.
E-mail: chfeng@scut.edu.cn (C.H. Feng); 201720141879@mail.scut.edu.cn (W.J. Duan)

Electrocatalyst	Electrolyte	Power supply	Time	Nitrate reduction efficiency %	Selectivity%		Refs
					N_2	NH_4^+	
16Cu-NPC	40 mL of 5 mM NaCl + 0.05 M Na_2SO_4 + 50 mg L^{-1} $NaNO_3$-N	-2.1 V (*vs.* Hg/Hg_2SO_4)	9 h	100	67	/	[1]
Cu-N-C-800	0.05 M Na_2SO_4 + 50 mg L^{-1} $NaNO_3$-N	-1.3 V (*vs.* SCE)	12 h	100	17	78	[2]
Cu–Pd@N-OMC	20 mL of 0.02 mol L^{-1} NaCl + 0.1 M Na_2SO_4 + 100 mg L^{-1} $NaNO_3$-N	-1.3 V (*vs.* SCE)	20 h	91	97	/	[3]
4CuPd@DCL-MCS/CNTs	0.02 M NaCl + 0.1 M Na_2SO_4 + 100 mg N^{-1} $NaNO_3$-N	-1.3 V (*vs.* SCE)	24 h	92	91	/	[4]
Pd–Cu/PNC	20 mL of 0.1 mol/L NaCl + 0.1 M Na_2SO_4+30 mg L^{-1} $NaNO_3$-N	-1.3 V (*vs.* SCE)	24 h	97	83	/	[5]
Pd_4Cu_4@N-pC	simulated sanitary sewage	-1.3 V (*vs.* SCE)	24 h	95	80	/	[6]

[Table S1]

[Figures S1 ~ S21]

Table S1. Summary of metal-encapsulated carbon-based (M@C) catalysts for ENRR in the literature and this work.

PdCu NCs-NOMC	20 mL of 0.1 M Na_2SO_4 + 100 mg L^{-1} $NaNO_3$-N	-1.3 V (*vs.* SCE)	24 h	86	60	/	[7]
FeNC/MC-900	20 mL of 0.1 M Na_2SO_4 + 100 mg L^{-1} $NaNO_3$-N	-1.3 V (*vs.* SCE)	24 h	87	81	/	[8]
Fe@C	0.02 M NaCl+ 100 mg L^{-1} $NaNO_3$-N	-1.3 V (*vs.* SCE)	24 h	76	98	/	[9]
B-Fe NCs	0.02 mM NaCl + 0.02 mM Na_2SO_4 + 100 mg L $NaNO_3$-N	-1.3 V (*vs.* SCE)	24 h	80	99	/	[10]
nZVI@OMC	50 mL of 0.02 M NaCl + 50 mg L^{-1} $NaNO_3$-N	-1.3 V (*vs.* SCE)	24 h	65	74	/	[11]
FeN-NC-140	20 mL of 0.02 M NaCl + 0.1 M Na_2SO_4 + 100 mg L^{-1} $NaNO_3$-N	-1.3 V (*vs.* SCE)	24 h	91	91	/	[12]
CL-Fe@C	0.02 M NaCl + 100 mg L^{-1} $NaNO_3$-N	-1.3 V (*vs.* SCE)	48 h	54	98		[13]
Fe(20%)@N-C	0.05 M Na_2SO_4 +1 g L^{-1} NaCl +50 mg L^{-1} $NaNO_3$-N	-1.3 V (*vs.* SCE)	24 h	83	100	/	[14]
Fe/Fe_3C-NCNF-2	50 mL of 0.03 M NaCl + 0.01 M Na_2SO_4+ 100 mg L^{-1} $NaNO_3$-N	-1.3 V (*vs.* SCE)	12 h	2928.42 mg N/g Fe	100	/	[15]
FeNi/g-mesoC/NF	0.05 mol L^{-1} Na_2SO_4 + 50 mg L^{-1} $NaNO_3$-N	-1.3 V (*vs.* SCE)	24 h	88	71	29	[16]
CNTs@CNx@Ag	25 mL of 0.1 M Na_2SO_4 + 25 mg L^{-1} $NaNO_3$-N	-0.29 V (*vs.* RHE)	30 h	53	97	/	[17]
P-Co@NCNT/NF	100 mL of 50 mM Na_2SO_4 + 50 mg L^{-1} $NaNO_3$-N	10 mA cm^{-2}	3 h	37	8	92	**this work**
Co@NCL/CC	100 mL of 50 mM Na_2SO_4 + 50 mg L^{-1} $NaNO_3$-N	10 mA cm^{-2}	3 h	72	7	93	**this work**
Co@NCNT	100 mL of 50 mM Na_2SO_4 + 50 mg L^{-1} $NaNO_3$-N	10 mA cm^{-2}	3 h	96	9	91	**this work**
Co@NCNT	100 mL of 50 mM Na_2SO_4 + 50 mg L^{-1} $NaNO_3$-N+1.5 g L^{-1} NaCl	10 mA cm^{-2}	3 h	97	100	/	**this work**

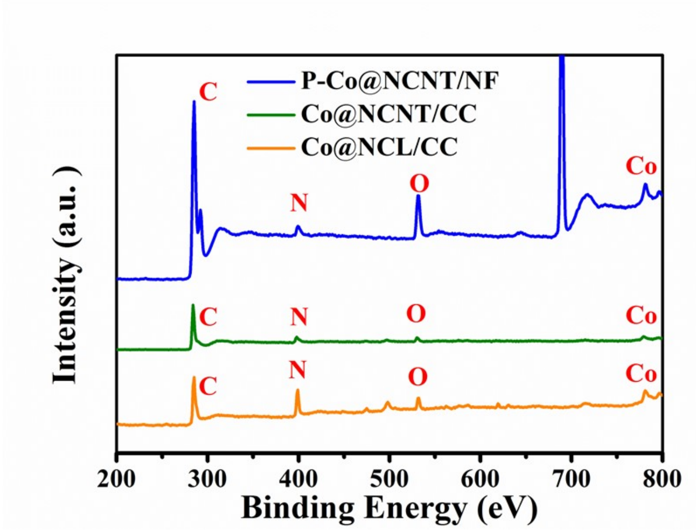

Fig. S1. XPS survey spectra of Co@NCNT/CC, Co@NCL/CC and P-Co@NCNT/NF.

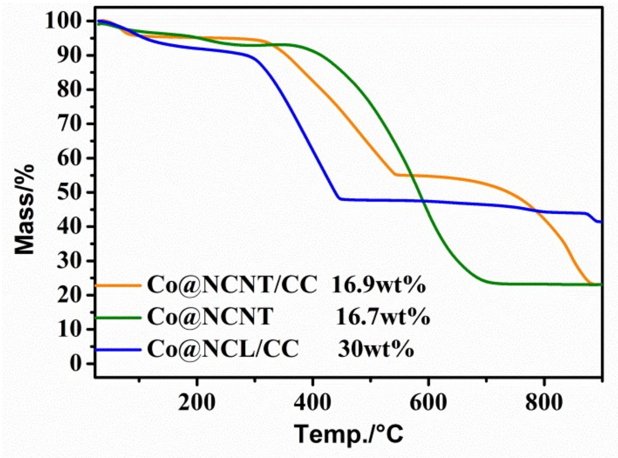

Fig. S2. TG analysis of three investigated catalysts.

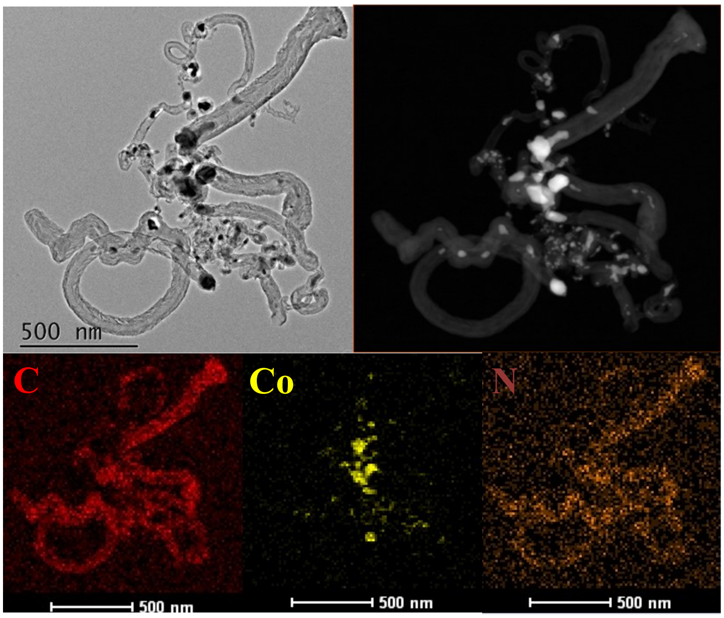

Fig. S3. HRTEM elemental mapping of Co@NCNT/CC.

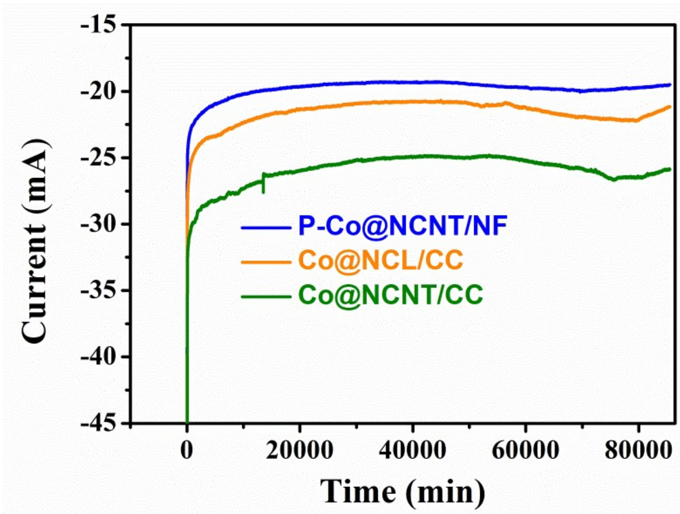

Fig. S4. I-t curves of three investigated catalysts at -1.3 V *vs.* SCE.

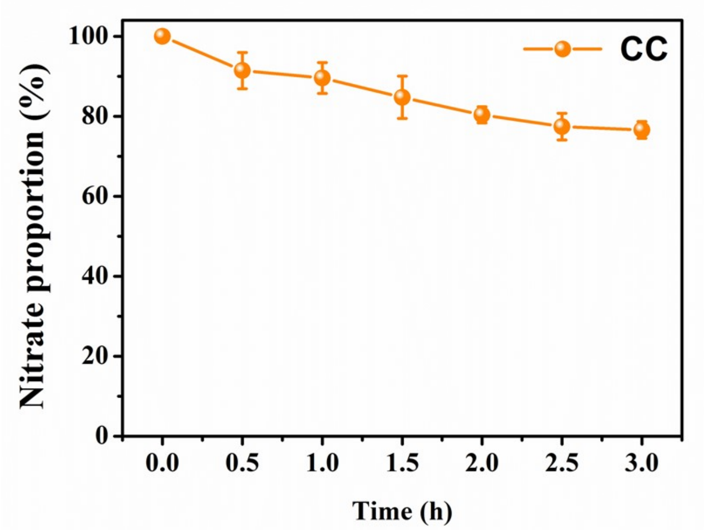

Fig. S5. Time courses of nitrate proportion for the pure CC towards ENRR. Experimental conditions: initial [NO_3^--N] = 50 mg L^{-1}, current density of 10 mA cm^{-2}, and electrolysis time of 3 h.

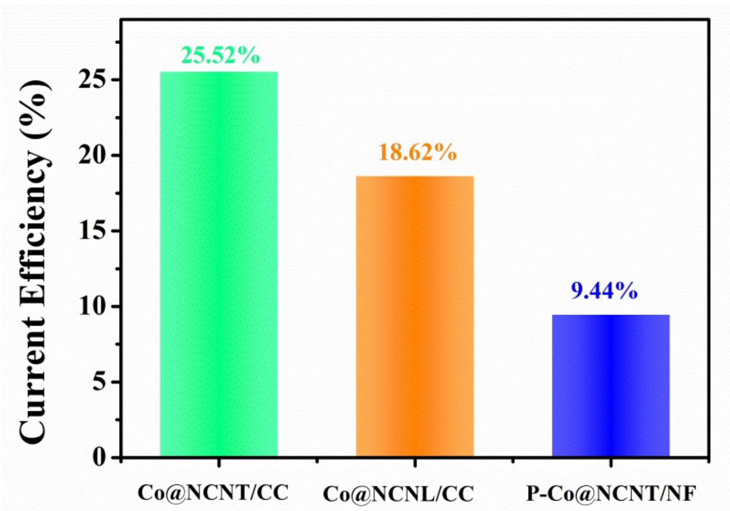

Fig. S6. Current efficiency CE(%) of three investigated electrodes for ENRR at 10 mA cm^{-2}.

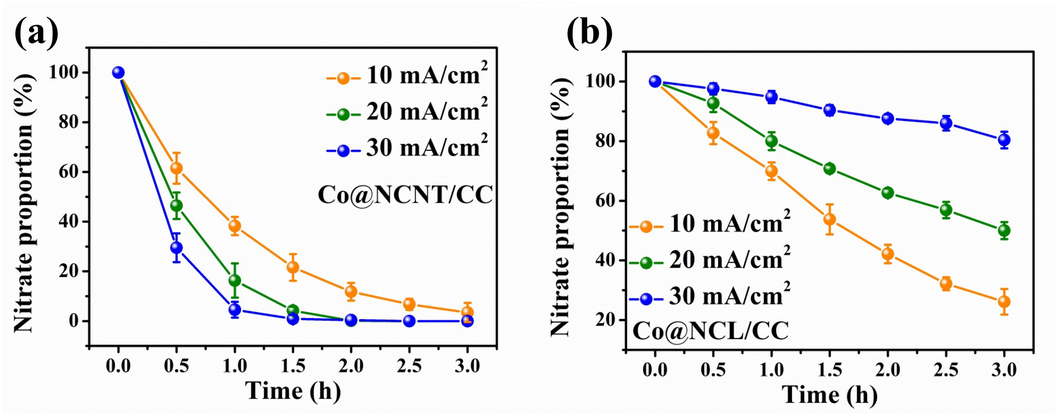

Fig. S7. Effect of current density on the ENRR performance of Co@NCNT/CC and Co@NCL/CC. Experimental conditions: initial [NO_3^--N] = 50 mg L^{-1}, 1.5 g L^{-1} NaCl, 100 mL of electrolyte, and initial pH = 7. 5.

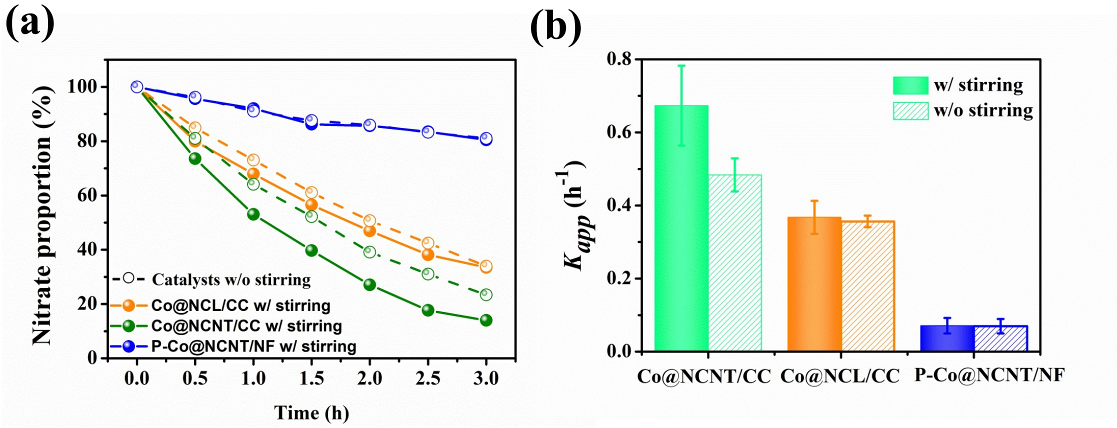

Fig. S8. Comparisons of (a) nitrate removal efficiency and (b) corresponding *Kapp* values of three catalysts during the stirring-control experiments. The initial concentration of NO_3^--N was 100 mg L^{-1}.

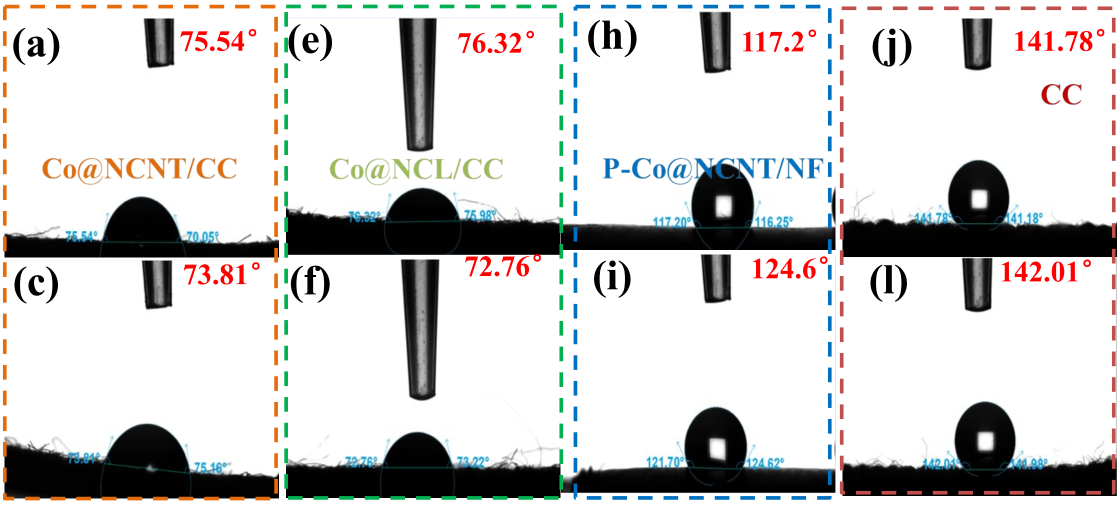

Fig. S9. Comparison of contact angles of the four samples.

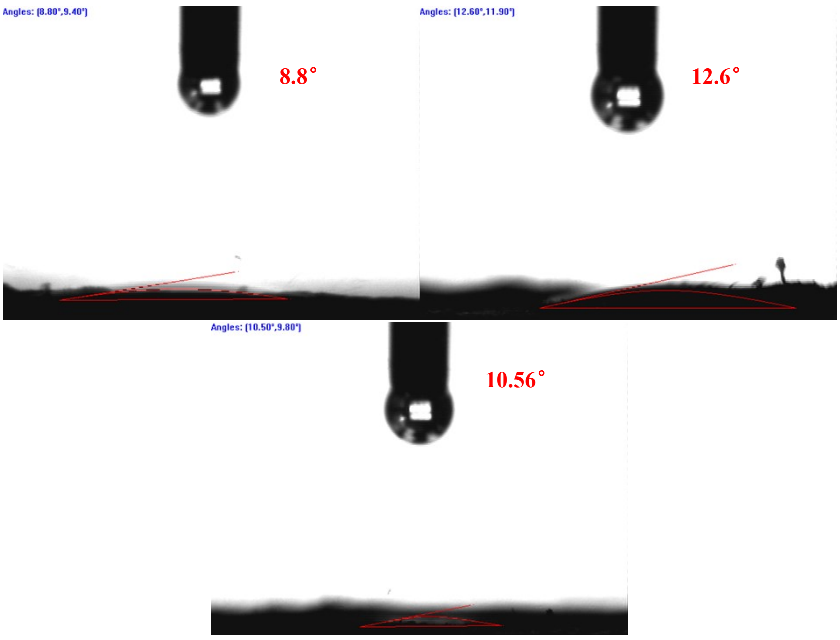

Fig. S10. Contact angles of P-Co@NCNT powders.

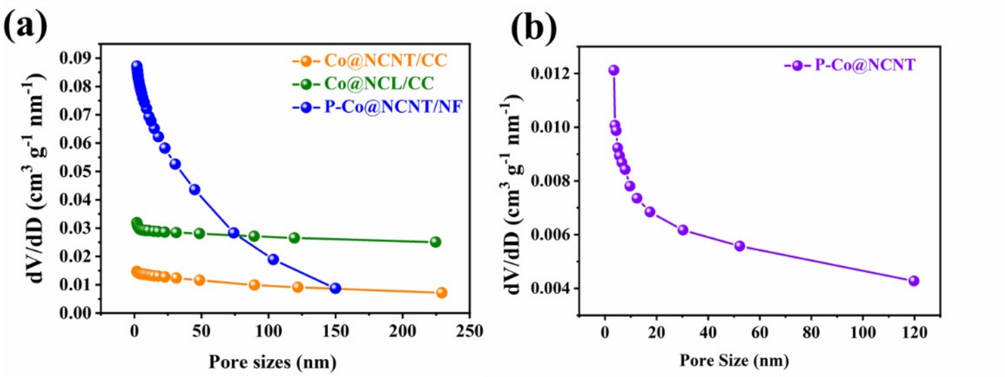

Fig. S11. N_2 adsorption−desorption isotherms and pore-size distributions of (a) three electrode samples and (b) P-Co@NCNT.

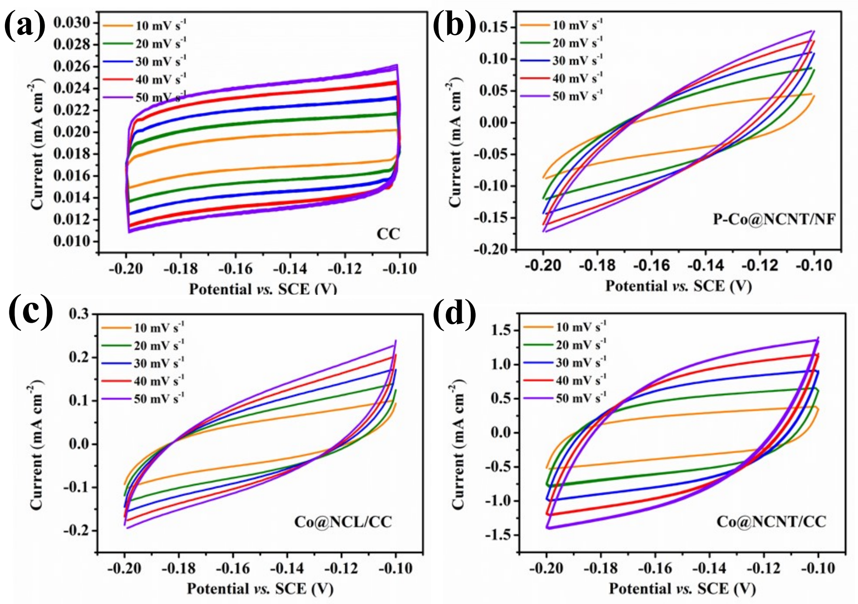

Fig. S12. CV curves of different electrode samples at various scan rates for identifying EASA.

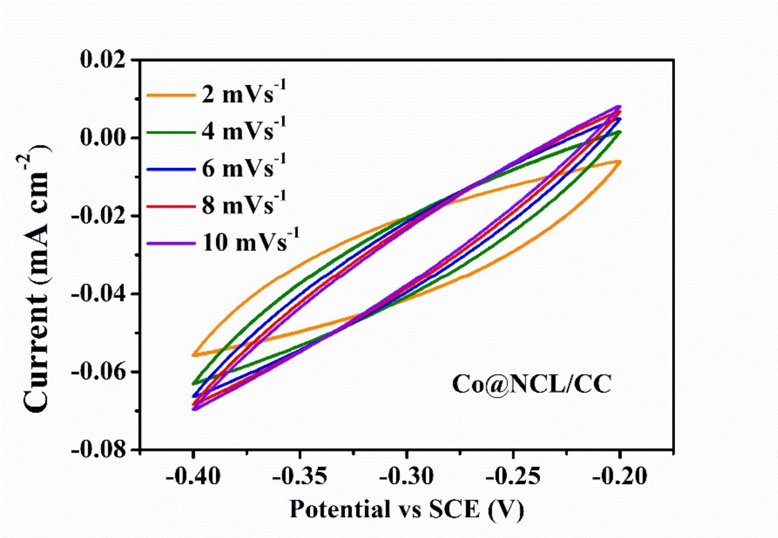

Fig. S13. CV curves of Co@NCL/CC at various scan rates recorded in 50 mg L^{-1} NO_3^--N and under N_2-saturated conditions.

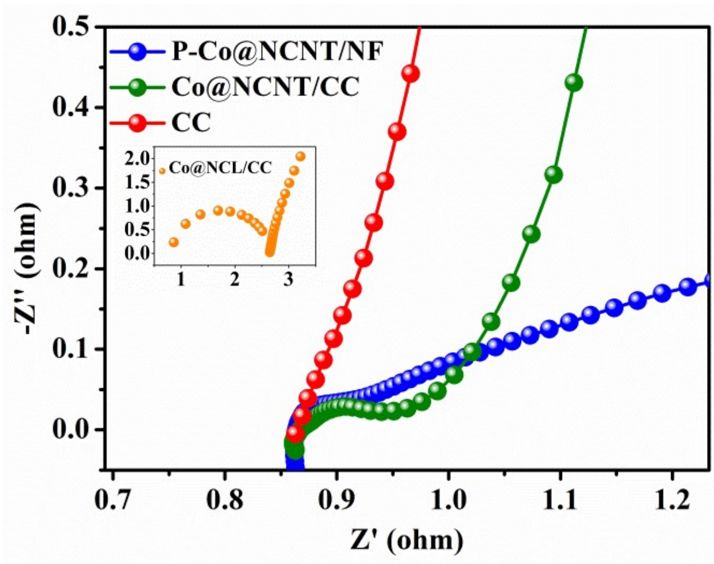

Fig. S14. EIS spectra of all investigated electrodes.

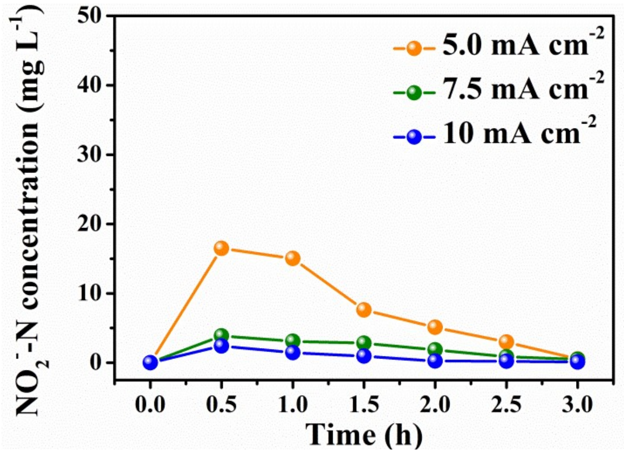

Fig. S15. Time courses of NO_2^--N concentration for ENRR on Co@NCNT/CC as a function of current density.

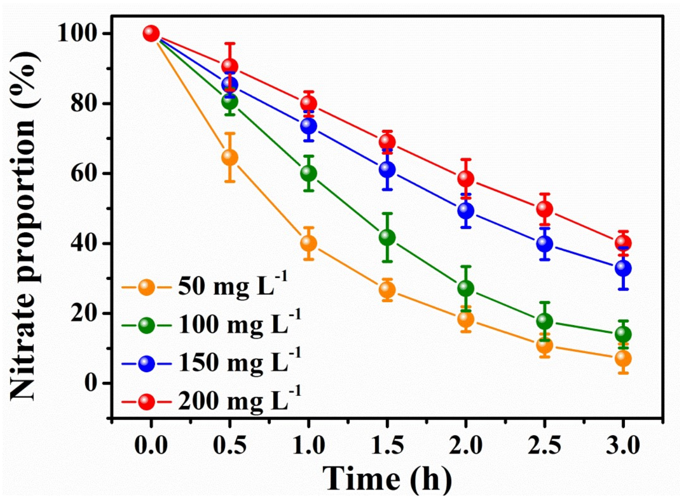

Fig. S16. Effect of initial nitrate concentration on the ENRR performance of Co@NCNT/CC. Experimental conditions: 1.5 g L^{-1} NaCl, 100 mL of electrolyte, 10 mA cm^{-2} current density, and initial pH = 7. 50.

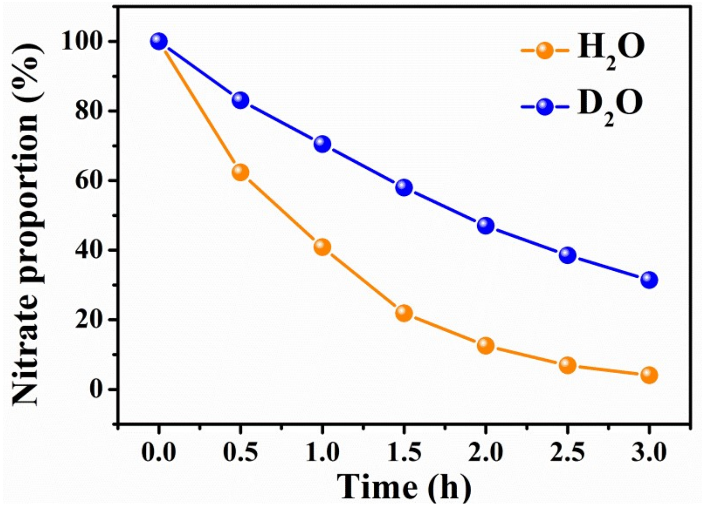

Fig. S17. Effect of D_2O replacement on the ENRR performance of Co@NCNT/CC. Experimental conditions: 1.5 g L^{-1} NaCl, 100 mL of electrolyte, 10 mA cm^{-2} current density, and initial pH = 7.50.

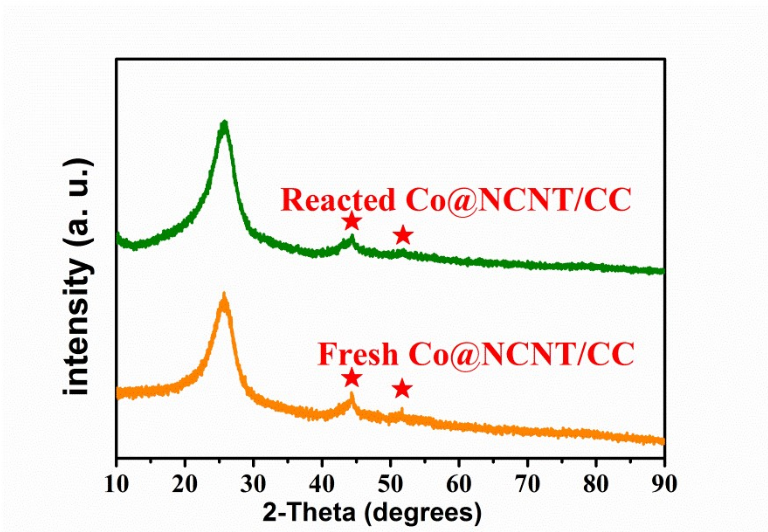

Fig. S18. XRD patterns of fresh and reacted Co@NCNT/CC (after 30 cycles).

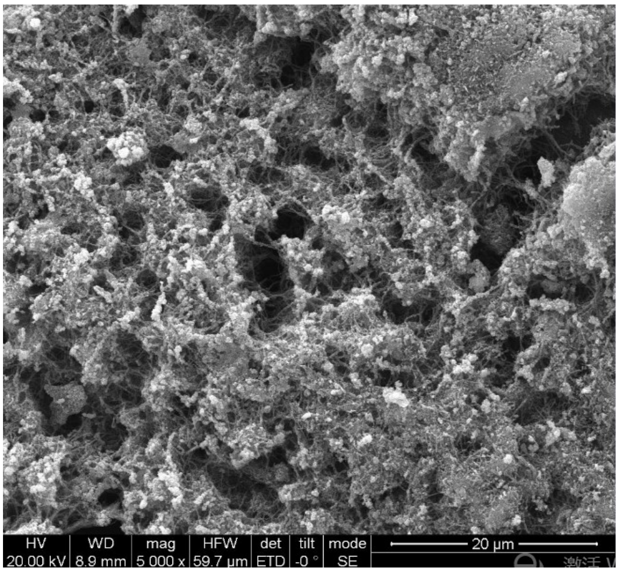

Fig. S19. SEM image of reacted Co@NCNT/CC (after 30 cycles).

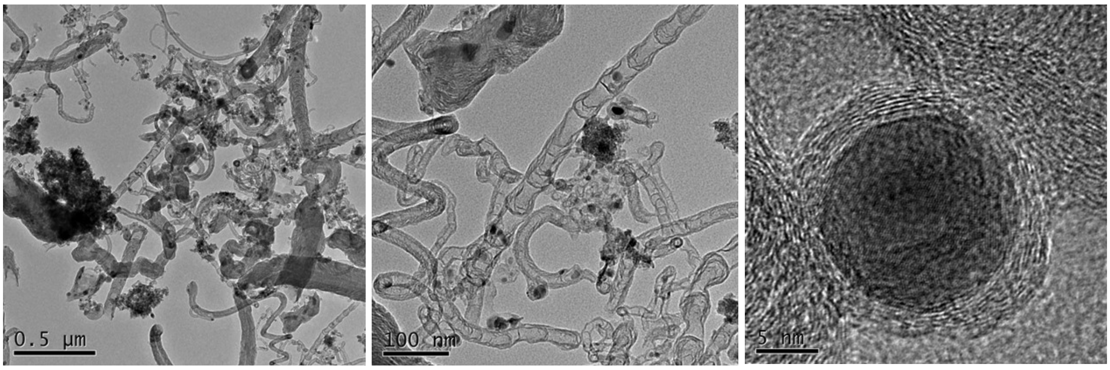

Fig. S20. HRTEM images of reacted Co@NCNT/CC (after 30 cycles) at different magnifications.

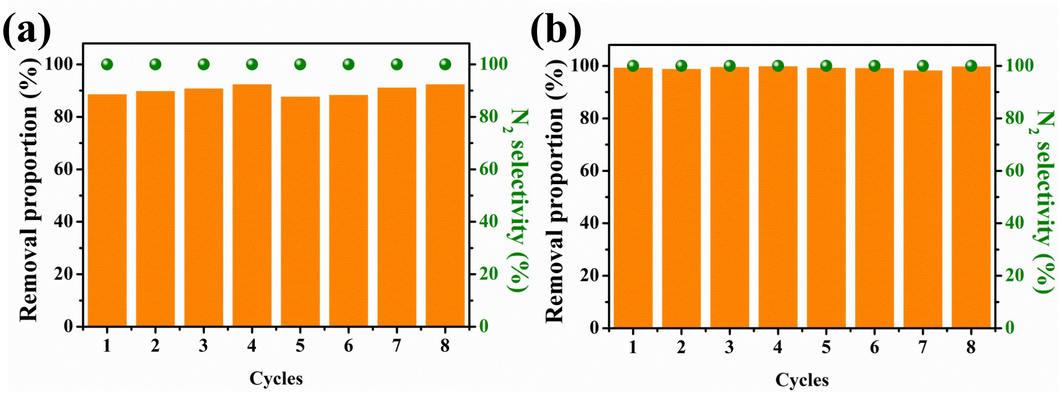

Fig. S21. Long-term operation stability of Co@NCNT/CC for ENRR at an initial pH of (a) 3 and (b) 14. Reaction conditions: electrolyte containing 50 mg L^{-1} NO_3^--N, 50 mM Na_2SO_4, and 1.5 g L^{-1} NaCl; current density of 10 mA cm^{-2}; and electrolysis of 3 h.

References:

1 X. Zhao, K. Zhao, X. Quan, S. Chen, H. Yu, Z. Zhang, J. Niu and S. Zhang, Efficient electrochemical nitrate removal on Cu and nitrogen doped carbon, *Chem. Eng. J.*, 2021, **415**, 128958.

2 T. Zhu, Q. Chen, P. Liao, W. Duan, S. Liang, Z. Yan and C. Feng, Single-atom Cu catalysts for enhanced electrocatalytic nitrate reduction with significant alleviation of nitrite production, *Small*, 2020, **16**, 2004526.

3 J. Wang, W. Teng, L. Ling, J. Fan, W.-x. Zhang and Z. Deng, Nanodenitrification with bimetallic nanoparticles confined in N-doped mesoporous carbon, *Environ. Sci.: Nano*, 2020, **7**, 1496-1506.

4 H. Xu, J. Wu, W. Luo, Q. Li, W. Zhang and J. Yang, Dendritic cell-inspired designed architectures toward highly efficient electrocatalysts for nitrate reduction reaction, *Small*, 2020, **16**, 2001775.

5 T. Gu, W. Teng, N. Bai, Z. Chen, J. Fan, W.-x. Zhang and D. Zhao, Nano-spatially confined Pd–Cu bimetals in porous N-doped carbon as an electrocatalyst for selective denitrification, *J. Mater. Chem. A*, 2020, **8**, 9545-9553.

6 M. Chen, H. Wang, Y. Zhao, W. Luo, L. Li, Z. Bian, L. Wang, W. Jiang and J. Yang, Achieving high-performance nitrate electrocatalysis with PdCu nanoparticles confined in nitrogen-doped carbon coralline, *Nanoscale*, 2018, **10**, 19023-19030.

7 H. Xu, H. Xu, Z. Chen, X. Ran, J. Fan, W. Luo, Z. Bian, W.-x. Zhang and J. Yang, Bimetallic PdCu nanocrystals immobilized by nitrogen-containing ordered mesoporous carbon for electrocatalytic denitrification, *ACS Appl. Mater. Interfaces*, 2019, **11**, 3861-3868.

8 W. Teng, J. Fan and W.-x. Zhang, Iron-catalyzed selective Ddenitrification over N-doped mesoporous carbon, *ACS Appl. Mater. Interfaces*, 2020, **12**, 28091-28099.

9 W. Hong, L. Su, J. Wang, M. Jiang, Y. Ma and J. Yang, Boosting the electrocatalysis of nitrate to nitrogen with iron nanoparticles embedded in carbon microspheres, *Chem. Commun.*, 2020, **56**, 14685-14688.

10 F. Ni, Y. Ma, J. Chen, W. Luo and J. Yang, Boron-iron nanochains for selective electrocatalytic reduction of nitrate, *Chin. Chem. Lett.*, 2021, **32**, 2073-2078.

11 W. Teng, N. Bai, Y. Liu, Y. Liu, J. Fan and W.-x. Zhang, Selective Nitrate reduction to dinitrogen by electrocatalysis on nanoscale iron encapsulated in mesoporous carbon, *Environ. Sci. Technol.*, 2018, **52**, 230-236.

12 J. Wang, L. Ling, Z. Deng and W.-x. Zhang, Nitrogen-doped iron for selective catalytic reduction of nitrate to dinitrogen, *Science Bulletin*, 2020, **65**, 926-933.

13 L. Su, D. Han, G. Zhu, H. Xu, W. Luo, L. Wang, W. Jiang, A. Dong and J. Yang, Tailoring the assembly of iron nanoparticles in carbon microspheres toward high-performance electrocatalytic denitrification, *Nano Lett.*, 2019, **19**, 5423-5430.

14 W. Duan, G. Li, Z. Lei, T. Zhu, Y. Xue, C. Wei and C. Feng, Highly active and durable carbon electrocatalyst for nitrate reduction reaction, *Water Res.*, 2019, **161**, 126-135.

15 Y. Lan, J. Chen, H. Zhang, W.-x. Zhang and J. Yang, Fe/Fe_3C nanoparticle-decorated N-doped carbon nanofibers for improving the nitrogen selectivity of electrocatalytic nitrate reduction, *J. Mater. Chem. A*, 2020, **8**, 15853-15863.

16 X. Chen, T. Zhang, M. Kan, D. Song, J. Jia, Y. Zhao and X. Qian, Binderless and oxygen vacancies rich FeNi/graphitized mesoporous carbon/Ni foam for electrocatalytic reduction of nitrate, *Environ. Sci. Technol.*, 2020, **54**, 13344-13353.

17 J. Liu, T. Cheng, L. Jiang, A. Kong and Y. Shan, Efficient nitrate reduction over novel covalent Ag-salophen polymer-derived "vein-leaf-apple"-like Ag@carbon structures, *ACS Appl. Mater. Interfaces*, 2020, **12**, 33186-33195.